

## Squeezing Maxwell's Equations into the Nanoscale

Diego M. Solís<sup>1</sup>, José M. Taboada<sup>2, \*</sup>, Luis Landesa<sup>2</sup>,  
José L. Rodríguez<sup>1</sup>, and Fernando Obelleiro<sup>1</sup>

*(Invited Paper)*

**Abstract**—The plasmonic behavior of nanostructured materials has ignited intense research for the fundamental physics of plasmonic structures and their cutting-edge applications concerning the fields of nanoscience and biosensing. The optical response of plasmonic metals is generally well-described by classical Maxwell's Equations (ME). Thus, the understanding of plasmons and the design of plasmonic nanostructures can therefore directly benefit from latest advances achieved in classic research areas such as computational electromagnetics. In this context, this paper is devoted to review the most recent advances in nanoplasmonic modeling, related with the latest breakthroughs in surface integral equation (SIE) formulations derived from ME. These works have extended the scope of application of Maxwell's Equations, from microwave/millimeter waves to infrared and optical frequency bands, in the emerging fields of nanoscience and medical biosensing.

### 1. INTRODUCTION

The great potential of metal/dielectric interfaces and, in particular, metallic nanoparticles (NP) to provide subwavelength confinement, enhancement, and spatiotemporal control of light, has put the field of plasmonics and nanoplasmonics at the forefront of nanotechnology research in the past years, up to the point that plasmonics is considered to be one of the 23 milestones in the history of photonics [1]. This rise of plasmonics has materialized in cutting-edge applications to medicine (e.g., cancer therapy) [2], nanoscale optical microscopy and lithography [3], molecular spectroscopy enhancement [4], photovoltaics [5], nanolasing [6], quantum processing [7], and wireless optical communications [8].

The optical response of metals is quite different from the high conductivity observed at lower frequencies. At optical frequencies the response is ruled by the plasma-like collective oscillations of the conduction electrons induced by the interaction of electromagnetic radiations [9, 10]. Intuitively, the conduction-electron gas of an irradiated metallic nanoparticle reacts toward the incident electric field and produce a net charge displacement from the equilibrium position, subsequently experiencing the restoring force from the positive ionic lattice. Additionally, electrons have an effective mass that causes them to react with increasing phase lag to the oscillating incident field as the frequency increases. This leads to plasmon collective oscillations, whose resonances are strongly governed by particle shape, size, composition and the dielectric properties of the metal itself and the background medium, and typically they are located in the visible and near-infrared (vis-NIR) regimes.

Plasmons are bosonic elementary excitations in a metallic solid and, in this regard, the question arises as to whether we should treat them in terms of a quantum-mechanical or a classical model. In other words, at which point is it justified that we neglect the discrete photon nature of the electromagnetic

---

*Received 1 November 2015, Accepted 10 November 2015, Scheduled 19 November 2015*

Invited paper for the Commemorative Collection on the 150-Year Anniversary of Maxwell's Equations.

\* Corresponding author: Jose Manuel Taboada (tabo@unex.es).

<sup>1</sup> Departamento de Teoría do Sinal e Comunicacóns, Universidade de Vigo, Pontevedra 36301, Spain. <sup>2</sup> Departamento de Tecnología de los Computadores y de las Comunicaciones, Universidad de Extremadura, Cáceres 10003, Spain.

waves and move from quantum electrodynamics over to Maxwell's classical theory? The answer is virtually always in the macroscopic phenomena domain. The classical notion of electromagnetic fields can be thought of as the classical limit (limit of large photon numbers and small momentum and energy transfers) of quantum electrodynamics [11]. If applicable, which is true for the linear response of metallic nanoparticles, it is possible to relate, via the fluctuation-dissipation theorem, the dielectric response to the dyadic Green tensor of Maxwell's theory, embodying all the details of the metal electrodynamics in the dielectric function (permittivity). In doing so, we are concealing the quantum-mechanical properties of matter within their dielectric description, which can be experimentally obtained [12, 13]. Simply put, we are transitioning from the microscopic world through the constitutive parameters  $\varepsilon$  and  $\mu$ . Remarkably, such a classical approach produces predictive results for particle and surface feature sizes down to around 1 nm, a distance below which nonlocal effects become significant [14].

Consequently, Maxwell's solvers can be applied safely in plasmonics, and as far as these solvers is concerned, plasmonic nanoparticles can be treated as regular homogeneous dielectrics. Thereby, they are entirely characterized by their permittivity (as they are non-magnetic), despite the underlying physics being in the antipodes of what might be expected for a dielectric in its very traditional definition. There are several popular methods that are capable of yielding rigorous classical electromagnetic solutions in arbitrary dielectric geometries. In particular, volume approaches such as the discrete-dipole approximation (DDA) [15], the finite difference in the time domain (FDTD) [16, 17], and frequency-domain finite-element methods (FEM) [18, 19] benefit from non-excessively complex parameterizations from the differential Maxwell's equations. However, as they must permeate the whole of space, they require solving a linear set of equations with a numerical demand scaling with at least the square of the volume. Although these approaches are increasingly popular, partly due to the availability of commercial software, dealing with realistic structures spanning several wavelengths in size rapidly inflates the computational costs required. Hence, the precise analysis of extended three-dimensional (3D) plasmonic systems using volumetric approaches still often exceeds current computational limits.

A more computationally efficient approach comprises the use of surface integral equation (SIE) formulations combined with the variational enforcement of the boundary conditions offered by the method of moments (MoM) [20–22]. These methods bring important advantages when compared to the above-mentioned volumetric approaches. As they are boundary integral equation (BIE) methods, they only require a parameterization of the boundary surfaces involved, rather than a 3D space embedding of the material structure and the volume of the structure itself, thus resulting in a dramatic reduction in the number of unknowns. Furthermore, no absorbing boundary conditions or surrounding empty space need to be specifically handled. This results in a great efficiency and versatility, which together with its high accuracy, has made the SIE-MoM approach becomes a pervasive technique for the solution of all kind of radiation and scattering problems in radiofrequency and microwaves.

Much as in the lower frequency bands, the availability of such efficient BIE Maxwell's solvers is very welcomed in optics. They enable the accurate simulation of larger plasmonic systems, assisting in the interpretation of experimental results [22]. They can also provide a priori information that reliably predicts the optical response from complex plasmonic assemblies, aiding the devise of new systems and increasing the possibilities for new fruitful discoveries [23].

In this paper, we present a deep review of the effort we have made over the last years extending the SIE-MoM [21, 24–26] combined with the most recent advances in spectral acceleration techniques, based on the multilevel fast multipole algorithm (MLFMA) [27–29] and the fast Fourier transform (FFT) [30–32], for the simulation of realistic large-scale plasmonic systems. This methodology was applied for the solution of problems such as the design of nanoantennas [33, 34] and optical wireless interconnects [35]. But among all the possible applications, we have concerned ourselves especially with biosensing, and particularly with surface enhanced Raman scattering (SERS) based spectroscopy [23, 36–38].

## 2. OPTICAL PROPERTIES OF METALS

The optical response of noble metals in the frequency domain is described by a dispersive complex dielectric function,  $\varepsilon(\omega)$ . From a qualitative point of view we can identify two mechanisms that contribute to  $\varepsilon(\omega)$ :

- Response of conduction electrons: From the concept of single electrons moving against a background

lattice of positive ion cores we can describe many of the fundamental electronic properties of the solid state. If, in a first naive approximation and for the sake of getting an intuitive picture, we ignore the lattice potential and electron-electron interactions, we end up with a gas of free electrons in the metal that can be treated as an electron liquid of high density or plasma. Drude adopted this classical approach to describe the electron dynamics in a metal [39], and came up with the motion equation of a damped oscillator, where the electrons, subjected to an incident electric field, move between heavier relatively immobile ions:

$$m\ddot{\mathbf{x}} + m\gamma\dot{\mathbf{x}} = -e\mathbf{E}. \quad (1)$$

This is known as Drude-Sommerfeld model (or simply Drude model) of the free electron gas, where  $\mathbf{x}$  is the displacement of the electron with respect to its rest position ( $\dot{\mathbf{x}}$  and  $\ddot{\mathbf{x}}$  represent the first and second time derivatives, respectively),  $m$  is its effective optical mass (incorporating some aspects of the band structure),  $e$  is its charge, and  $\gamma = 1/\tau$  is a motion damping factor accounting for collisions, being  $\tau$  the relaxation time of the free electron gas. If a time harmonic variation  $\exp(j\omega t)$  is assumed, and jumping over to the Fourier transformed space, this can be solved as:

$$\mathbf{x} = \frac{e}{m(\omega^2 - j\gamma\omega)}\mathbf{E}, \quad (2)$$

which allows to use a linear dielectric model that leads to a total polarization  $\mathbf{P}$  of the material equal to  $\mathbf{P} = n\mathbf{p} = -nex$ , being  $n$  the electrons per unit volume and  $\mathbf{p}$  the dipole moment produced by a single electron. It is then straightforward to derive the desired relative dielectric function:

$$\varepsilon(\omega) = 1 - \frac{\omega_p^2}{\omega^2 - j\gamma\omega}, \quad (3)$$

where  $\omega_p = \sqrt{ne^2/\varepsilon_0 m}$  is the volume plasma frequency, with values lying in the ultraviolet region for most metals,  $\varepsilon_0$  being the permittivity of vacuum. The requirement of metallic character entails that  $\text{Re}\{\varepsilon(\omega)\} < 0$ , a condition that metals fulfill at frequencies below the bulk plasmon frequency  $\omega_p$ , and which allows, as we will see below, the existence of surface plasmons.

For the noble metals, an extension to this model is needed in the region  $\omega > \omega_p$  (with a response dominated by free  $s$  electrons) that includes the residual polarization due to the positive background of the ion cores. This is done by introducing the dielectric constant  $\varepsilon_\infty$ , corresponding to the limiting value of  $\varepsilon(\omega \rightarrow \infty)$ , so that:

$$\varepsilon(\omega) = \varepsilon_\infty - \frac{\omega_p^2}{\omega^2 - j\gamma\omega}. \quad (4)$$

- Response of valence (bound) electrons: The dielectric function of the Drude model adequately describes the optical response of metals only for photon energies below the threshold of transitions between electronic bands. Above this threshold, higher-energy photons can promote bound electrons from lower-lying d-bands into the conduction band. For some of the noble metals, interband effects already start to occur for energies over 1 eV (corresponding to a wavelength  $\lambda \approx 1 \mu\text{m}$ ), which invalidates the adequacy of this model at high frequencies. This inadequate modeling can be overcome by replacing Equation (1) by:

$$m\ddot{\mathbf{x}} + m\gamma\dot{\mathbf{x}} + m\omega_0^2\mathbf{x} = -e\mathbf{E}, \quad (5)$$

which describes interband transitions through the classical picture of a bound electron with resonance frequency  $\omega_0$ . An accurate model for  $\varepsilon(\omega)$  requires the solution of several of these equations, each equation yielding a separate polarization that translates into a Lorentz-oscillator term, to be added to Equation (4), of the form [40]:

$$\frac{A_i}{\omega_{0,i}^2 - \omega^2 + j\gamma_i\omega}, \quad (6)$$

where  $\omega_{0,i}$  and  $\gamma_i$  are the plasma and the damping frequencies for the bound electrons, and  $A_i$  is a parameter that weights the contribution of the  $i$ -th interband transition to the dielectric function.

The previous expressions provide a good insight into optical properties of metals. Let's describe now the interaction between a metal and an incident light.

## 2.1. Surface Plasmon Polariton

When an electromagnetic wave impinges on a metal, a force is applied on the conduction electrons' charges, which show such little resistance that their movement easily follows the driving electromagnetic field at low frequencies. This movement of charges in turn creates a scattered field, which cancels the electromagnetic field inside the metal. This is why, for radiofrequency and microwave applications, metals are usually modeled using the perfect conductor approximation. In the optical regime, nonetheless, the electron movement lags behind the rapidly varying electromagnetic field, allowing for a reduced screening effect, and hence a non-negligible penetration depth of the field into the metal.

In certain cases, if the relation of metallo-dielectric permittivities fulfills certain criteria, the electrons' collective motion induces an electromagnetic field near the surface capable of maintaining by itself the collective electron motions, generating a self-sustained excitation which may propagate closely confined along the metal's surface. This excitation is called a surface plasmon polariton (SPP), and was first theoretically investigated by Ritchie in the context of loss spectra of low-energy electron beams undergoing diffraction at thin metallic films [41]. The simplest geometry capable of sustaining SPPs is a planar interface between a metal ( $z < 0$ ) with dielectric function  $\varepsilon_1(\omega)$  and a non-absorbing half space ( $z > 0$ ) with positive real dielectric constant  $\varepsilon_2(\omega)$ . We seek homogeneous propagating wave solutions confined to the interface (evanescent decay in the perpendicular  $z$ -direction). The Helmholtz wave equation

$$(\nabla^2 + \varepsilon k_0^2) \mathbf{E} = 0 \quad (7)$$

has then to be solved separately in each half-space, and the enforcement of the boundary conditions will match both solutions at the interface. This supports two sets of self-consistent solutions with different polarization properties, TE ( $s$ -polarized) and TM ( $p$ -polarized), but it can be shown [10] that the first do not excite surface modes, so we will focus on the latter:

$$\mathbf{E}_i = (E_{x,i}\hat{x} + E_{z,i}\hat{z})e^{-jk_x x}e^{-jk_{z,i} z}, \quad (8)$$

with  $i = 1, 2$ . Note that the component of the wave vector parallel to the interface,  $k_x$ , is the same for both regions. As the relation below holds:

$$k_x^2 + k_{z,i}^2 = \varepsilon_i k_0^2, \quad (9)$$

and applying Gauss's law, we have:

$$k_x E_{x,i} + k_{z,i} E_{z,i} = 0, \quad (10)$$

such that we can rewrite Equation (8) as:

$$\mathbf{E}_i = (\hat{x} - k_x/k_{z,i}\hat{z})e^{-jk_x x}e^{-jk_{z,i} z}. \quad (11)$$

Continuity of  $E_x$  and  $D_z$  at the interface requires that  $E_{x,1} = E_{x,2}$  and  $\varepsilon_1 E_{z,1} = \varepsilon_2 E_{z,2}$ . The existence of a solution then requires that  $\varepsilon_1 k_{z,2} = \varepsilon_2 k_{z,1}$ , which leads to the dispersion relation between the wavevector components of SPPs and the angular frequency  $\omega$ :

$$k_x = \frac{\omega}{c} \sqrt{\frac{\varepsilon_1 \varepsilon_2}{\varepsilon_1 + \varepsilon_2}}, \quad (12)$$

$$k_{z,i} = \frac{\omega}{c} \sqrt{\frac{\varepsilon_i^2}{\varepsilon_1 + \varepsilon_2}}. \quad (13)$$

In order to discuss the conditions necessary for an interface mode to exist, we may assume, for simplicity, that the metal is an ideal conductor with negligible  $\text{Im}\{\varepsilon_1\}$ . On the one hand, we are looking for interface waves that propagate along the surface, i.e., we require a real  $k_x$ ; this holds if the numerator and denominator in Equation (12) are either both positive or both negative. On the other hand, in order to obtain a bound or exponentially decaying solution, we need purely imaginary  $k_z$  in both media; this can only be fulfilled if the sum of the dielectric functions is negative. We thereby conclude that the conditions for an interface mode to exist are the following:

$$\varepsilon_1(\omega)\varepsilon_2(\omega) < 0, \quad (14)$$

$$\varepsilon_1(\omega) + \varepsilon_2(\omega) < 0. \quad (15)$$

Taking a closer look to the dispersion curves in Fig. 1 may provide some more valuable physical insight. We can clearly identify two well-differentiated sets of modes:

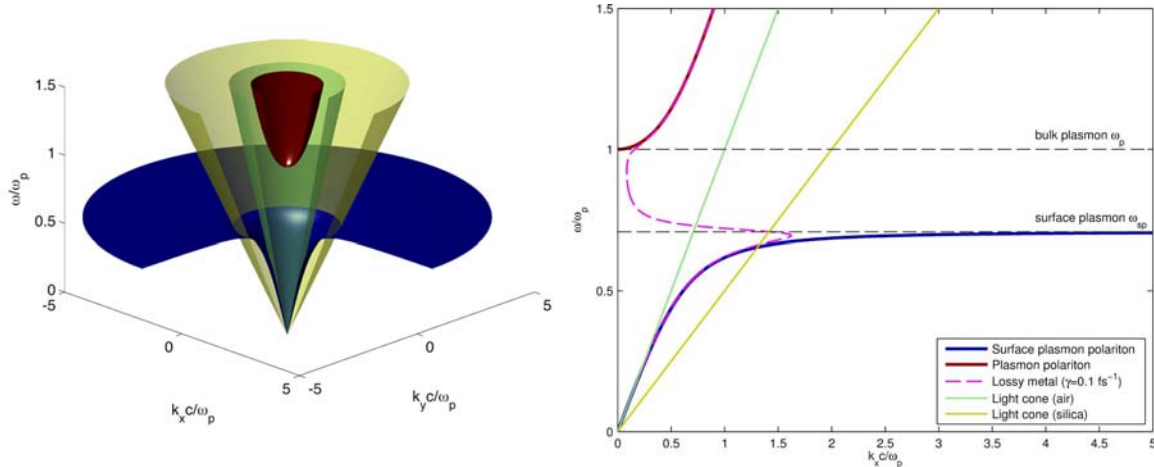


**Figure 1.** Dispersion relation of SPPs at the interface between a Drude metal with negligible collision frequency and air, together with the light dispersion for air and silica. Direct SPP coupling is only possible at the intersection between the SPP dispersion curve and the light cone of silica. The dispersion of SPPs corresponding to the lossy metal case is also included. The lower 3D plot illustrates the resulting dispersion surfaces if propagation in any direction of the  $xy$  interface is allowed.

- Bound modes (SPPs), which in the dispersion curves are lying to the right of the light cone. An example of SPP is shown in Fig. 2. Note that direct excitation of such modes with an electromagnetic wave would require the fulfillment of both energy and momentum conservation simultaneously, but this is not possible (light momentum  $k_0 \sin(\theta)$  is always too small, being  $\theta$  the tilt angle of the direction of incidence with respect to the interface’s normal) unless the missing momentum contribution is provided.
- Radiative modes, which transmit into the metal in the transparency regime  $\omega > \omega_p$ .
- Between the regime of the bound and radiative modes, a frequency gap region with purely imaginary  $k_x$  prohibiting propagation exists.

Regarding bound modes, for small wave vectors corresponding to low (mid-infrared or lower) frequencies,  $k_x$  is close to  $k_0$  of the light cone, with SPP waves extending over many wavelengths into the dielectric space (Sommerfeld-Zenneck waves), similar in nature to a grazing-incidence light field. On the contrary, for large wave vectors, the frequency of the SPPs approaches the characteristic surface plasmon frequency:

$$\omega_{sp} = \frac{\omega_p}{\sqrt{1 + \epsilon_2}}, \tag{16}$$

obtained through the insertion of the Drude-model dielectric function into Equation (11). In the limit of negligible damping of the conduction electron oscillation (implying  $\text{Im}\{\epsilon_1(\omega)\} = 0$ ), the wave vector  $k_x$  goes to infinity as the frequency approaches  $\omega_{sp}$ , and the group velocity  $v_g \rightarrow 0$ . This mode, known as surface plasmon, thus acquires electrostatic character.

However, as excitations of the conduction electrons of real metals suffer both from free-electron and interband damping,  $\epsilon_1(\omega)$  is actually complex, and also the SPP propagation constant  $k_x$ . Thus, the traveling SPPs have a wavelength of  $2\pi/\text{Re}\{k_x\}$ , and are damped with an energy attenuation length (also called propagation length)  $L = 1/(2\text{Im}\{k_x\})$ , typically between 10 and 100  $\mu\text{m}$  in the visible. Besides, the SPP dispersion bends back into the radiation region, so the quasi-bound leaky part of the dispersion relation between  $\omega_{sp}$  and  $\omega_p$  is now allowed, in contrast to the case of an ideal conductor.

## 2.2. Localized Surface Plasmon Resonance

In the case of a finite metallic nanoparticle excited by an electromagnetic wave, its small size allows the conduction electrons to oscillate collectively with a restoring force coming from the particle’s

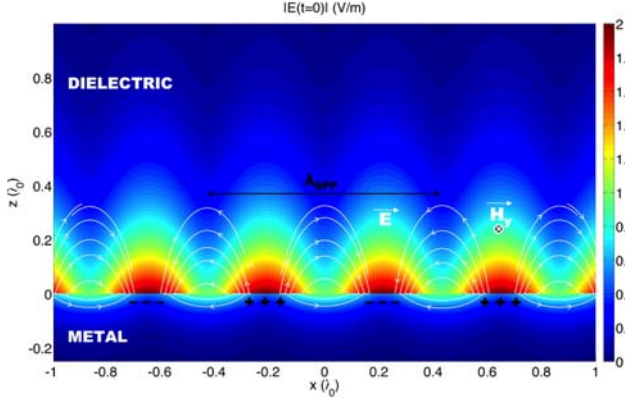


**Figure 2.** Near-field distribution for an SPP arising at a metal/dielectric interface with  $\varepsilon_1 = -4$  and  $\varepsilon_2 = 1$ .

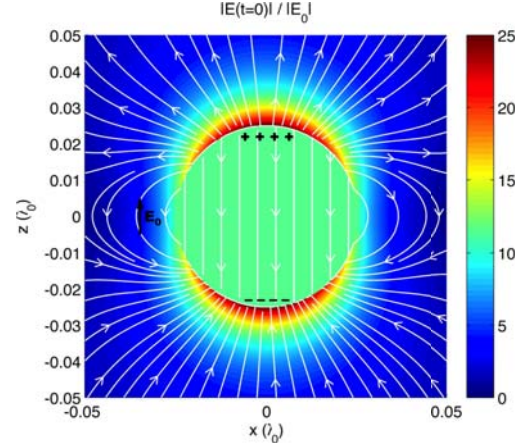


**Figure 3.** Near-field distribution of an LSPR obtained from the quasi-static limit for a sphere of radius  $\lambda_0 = 40$  and  $\varepsilon_1 = -4$ , immersed in water (refractive index  $n_2 = 1.33$ ) and irradiated by  $E_0 \hat{z}$ .

walls. As frequency increases, so does the phase lag of these collective oscillations with respect to the incident excitation, leading to plasmonic resonances when this phase lag equals  $\pi/2$  rad. These are not propagating resonances but rather localized to the nanoparticle, hence their denomination, localized surface plasmon resonance (LSPR). The resonance wavelength thus not only depends upon the constitutive parameters of the inner and outer regions, but also upon the particle size and shape.

The optical response of a particle of size  $d$  can be approximately analyzed through a simple quasi-static approximation, provided that  $d \ll \lambda$ . In that case, we are looking for a solution of the Laplace equation for the potential,  $\nabla^2 \Phi = 0$ , which will allow us to retrieve  $\mathbf{E} = -\nabla \Phi$ . If, for convenience, we assume a spherical geometry for the nanoparticle (radius  $a$ ), the solution to the problem for an incident electric static field  $\mathbf{E}_0 = E_0 \hat{z}$  can be obtained as [10, 11]:

$$\Phi_1(r, \theta) = -\frac{3\varepsilon_2}{\varepsilon_1 + 2\varepsilon_2} E_0 r \cos \theta, \quad (17)$$

$$\Phi_2(r, \theta) = -E_0 r \cos \theta + \frac{\varepsilon_1 - \varepsilon_2}{\varepsilon_1 + 2\varepsilon_2} E_0 a^3 \frac{\cos \theta}{r^2}, \quad (18)$$

for the inner and outer regions, respectively, with  $\theta$  defining the angle between the position vector  $\mathbf{r}$  and the  $z$ -axis. Equation (18) can be expressed as:

$$\Phi_2(r, \theta) = -E_0 r \cos \theta + \frac{\mathbf{p} \cdot \mathbf{r}}{4\pi\varepsilon_0\varepsilon_2 r^3}, \quad (19)$$

where we have inserted the particle's dipole moment  $\mathbf{p} = \varepsilon_0\varepsilon_2\alpha\mathbf{E}_0$ , being  $\alpha$  the polarizability:

$$\alpha = 4\pi a^3 \frac{\varepsilon_1 - \varepsilon_2}{\varepsilon_1 + 2\varepsilon_2}. \quad (20)$$

Of course, for larger particles retardation effects come into play and accurate full-wave electrodynamics solvers must be applied instead.

The previous equations lead to the well-known condition of plasmonic resonance for a very small nanosphere:

$$\text{Re} \{ \varepsilon_1(\omega) \} = -2\varepsilon_2. \quad (21)$$

A resonance for the polarizability leads to a field-enhancement for both the inner and outer regions, an important property most of the prominent plasmonic applications rely on. Fig. 3 shows an example of such LSPR on a plasmonic nanosphere. Note the field enhancement and confinement leading to strong hot spots in the outer region, as well as an appreciable penetration of field into the nanoparticle. Remarkably, LSPRs can be excited optically without the need for careful matching of the wavevector as in SPPs.

### 3. INTEGRAL EQUATION MAXWELL'S SOLVERS

#### 3.1. Method of Moments for Surface Integral Equations

Maxwell's surface integral equation formulations combined with the method of moments is a powerful tool that has demonstrated high accuracy and efficiency for the analysis of composite objects with real conductors and dielectrics in radio frequency and microwave regimes. Recently, it has successfully been extended to the solution of metamaterial and plasmonic problems in near infrared frequencies and in optics [21, 22, 24–26]. Based on Love's equivalence principle, metallic nanostructures can be replaced by equivalent electric and magnetic currents distributed over the boundary surfaces and interfaces. The total electromagnetic fields can be therefore obtained as a superposition of the known incident fields and the unknown scattered fields, which can be self-consistently obtained from the equivalent currents through the integro differential Stratton-Chu representation formulas and the 3D electrodynamic homogeneous Green's function.

More precisely, we derive a set of SIEs for the unknown equivalent currents by imposing the well-known continuity of the tangential fields at the boundaries. Among the infinitely many possibilities, we fulfill the procedure of [42], which has proven to render a set of stable and well-conditioned equations. Let us denote with  $S_{ij}$  (or  $S_{ji}$ ) the interface between two homogeneous regions  $R_i$  and  $R_j$ . In each region the electric field integral equation (EFIE) and the magnetic field integral equation (MFIE) can be formulated in two alternative ways, depending on the method applied to project the fields onto the surfaces: Namely, the tangential (T) and the twisted or normal (N) EFIE and MFIE. Combining these integral equations in region  $R_l$ , with  $l = i, j$ , we can derive the two following combined field integral equations (CFIEs) on  $S_{ij}$ :

$$a_l \frac{1}{\eta_l} \text{T-EFIE}_l + b_l \text{N-MFIE}_l, \quad (22)$$

$$-c_l \text{N-EFIE}_l + d_l \eta_l \text{T-MFIE}_l, \quad (23)$$

where  $\eta_l$  is the intrinsic impedance in region  $R_l$  and with  $a_l$ ,  $b_l$ ,  $c_l$  and  $d_l$  the appropriate complex combination coefficients in  $R_l$ . Usually these equations are referred to as the electric current (J) CFIE, and the magnetic current (M) CFIE, as the electric current and the magnetic current are respectively well-tested in each one. The two regions defining the interface  $S_{ij}$  are then mixed just by combining Equations (22) and (23) for regions  $R_i$  and  $R_j$ , yielding two single integral equations for the interface  $S_{ij}$  as follows:

$$\text{JCFIE}_i + \text{JCFIE}_j, \quad (24)$$

$$\text{MCFIE}_i + \text{MCFIE}_j. \quad (25)$$

These SIEs are subsequently discretized by applying the Galerkin MoM procedure [20] using a set of known basis and testing functions, leading to a dense matrix system of linear equations. In our case we use the well-known Rao-Wilton-Glisson (RWG) vector basis/testing functions [43], together with the analytical extraction procedures of [44–47] for the accurate evaluation of singular and hypersingular integrals that appear in Equations (24) and (25). This results in a linear system of  $N$  equations and  $N$  unknowns,  $N$  being the number of surface RWG basis functions used to expand the electric and magnetic currents, that can be written as follows:

$$\mathbf{Z} \cdot \mathbf{I} = \mathbf{V}. \quad (26)$$

In order to apply the SIE-MoM to the correct modeling of the optical properties of metals as described in the previous section, the only caveat is the proper derivation of electromagnetic parameters, namely the wavevector and the intrinsic impedance. Under the time-harmonic variation of  $\exp(j\omega t)$ , the constitutive parameters of a passive homogeneous region  $R_i$  fulfill the general form  $\varepsilon_i = \varepsilon'_i - j\varepsilon''_i$  and  $\mu_i = \mu'_i - j\mu''_i$ . In conventional materials,  $\varepsilon'_i$ ,  $\varepsilon''_i$ ,  $\mu'_i$ , and  $\mu''_i$  are positive quantities, and the derivations of the wave number  $k_i = \sqrt{\omega^2 \mu_i \varepsilon_i}$  and the wave impedance,  $\eta_i = \sqrt{\mu_i / \varepsilon_i}$ , do not suffer from any ambiguity. Nevertheless,  $\varepsilon'_i$  becomes negative when dealing with plasmonic media (while  $\mu'_i$  could become also negative in some metamaterials). In such cases we could face the ambiguities in the definition of  $k_i$  and  $\eta_i$  due to the presence of the square root, which is a multivalued function for complex arguments [48]. Obviously, only one solution is valid and obeys physical laws [49] such that  $\text{Re}\{\eta_i\} \geq 0$ ,

thus guaranteeing causality in the sense of energy flowing away from the source, and  $\text{Im}\{k_i\} \leq 0$ , leading to a stable system where the wave energy attenuates as it propagates away from the source in a lossy (passive) medium.

Under the C++ standard [50], the branch cut of the square-root function lies along the negative real axis, which limits the phase of the complex arguments to the interval  $(-\pi, \pi]$ , and the phase range of the square-root result (which is given in the principal-value sense) to  $(-\pi/2, \pi/2]$ . The ambiguity in the solution can be avoided by factorizing the wave parameters to un-wrap the phases of  $\varepsilon_i$  and  $\mu_i$ , as illustrated in the complex plane depicted in Fig. 4. Importantly, the lossless cases must be treated as limiting cases, defined from the general lossy case as the limit when the electric and/or magnetic losses approach zero. The above conditions pose the following expressions for the calculation of the wave parameters [51]:

$$k_i = \lim_{\delta \rightarrow 0} \omega \sqrt{\mu_i - j\delta} \sqrt{\varepsilon_i - j\delta}, \quad (27)$$

$$\eta_i = \lim_{\delta \rightarrow 0} \frac{\sqrt{\mu_i - j\delta}}{\sqrt{\varepsilon_i - j\delta}}. \quad (28)$$

Remarkably, the previous expressions yield valid solutions in all cases, including lossy cases where the addition of an infinitesimal imaginary part does not have any significant impact on the results.

Up to this point we are considering single interfaces between two media (e.g., a homogeneous particle in the background). Nonetheless, practical applications often comprise many homogeneous regions with different compositions touching each other. One leap forward of utmost importance is then to gain the ability to address multiple composite piecewise-homogeneous penetrable bodies. For this, one has to appropriately treat those edges or junctions where more than two regions meet, such that there are only two independent unknowns, one for the electric current  $\mathbf{J}$  and another for the magnetic current  $\mathbf{M}$ , since the unknown coefficients of the oriented vector basis functions supporting a given junction must have the same value. This can be looked at as the continuity property of surface currents at junctions, i.e., Kirchoff's laws for surface currents, that translates into the enforcement of field boundary condition across these multiple interfaces.

It is well-known that the implementation of such continuities in the framework of a SIE-MoM solver becomes rather tedious [52, 53]. An alternative simple way to handle this casuistic was proposed in [25], with the aid of so-called multiregion (MR) piecewise vector basis functions. The MR basis functions are oriented functions that implicitly satisfy the boundary conditions. They are defined similarly in both boundary surfaces and junctions, yielding a compact formulation that greatly simplifies the implementation of SIE-MoM when tackling scattering and/or radiation problems with composite

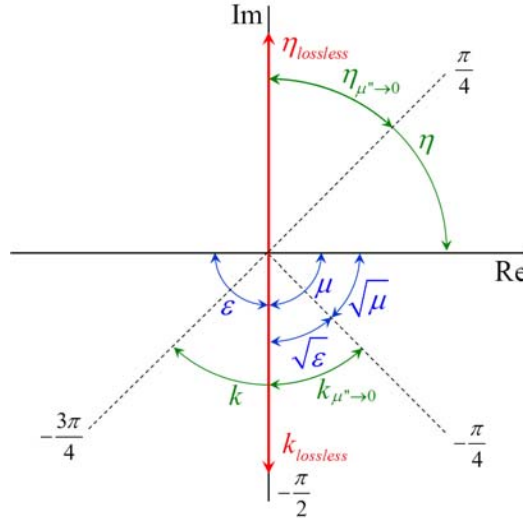


**Figure 4.** Complex diagram relating  $k$  and  $\eta$  to  $\varepsilon$  and  $\mu$ , and their respective square roots for plasmonic media.

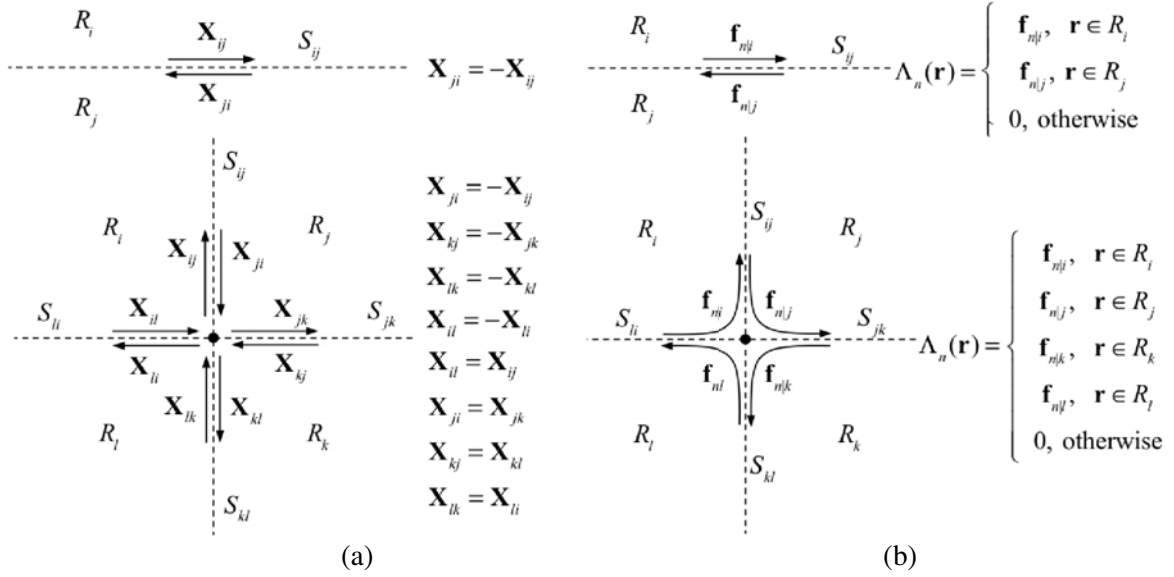


**Figure 5.** (a) Boundary conditions at interfaces (top) and junctions (bottom).  $\mathbf{X}$  stands for  $\mathbf{J}$  or  $\mathbf{M}$ . (b) Piecewise multiregion (MR) oriented basis functions  $\Lambda_n$  implicitly satisfying the boundary conditions at interfaces (top) and junctions (bottom).

objects with multiple junctions. Fig. 5(a) illustrates the boundary conditions ensuring the continuity of the tangential component of the fields at a boundary interface between two media (top) and at a junction between four regions (bottom). These conditions are directly satisfied by expanding the unknown equivalent currents in a sum of MR piecewise functions  $\Lambda_n$  as depicted in Fig. 5(b), where  $\mathbf{f}_{n|i}$  are subsectional basis/testing functions (RWG functions in our case) defined on each of the regions  $R_i$  that conform the interface or junction [25].

### 3.2. Acceleration Techniques

As noted above, SIE-MoM yields a relatively reduced numerical size with respect to volumetric approaches (2D vs 3D). It also provides a greater stability, as the field singularities and hotspots related for example to localized surface-plasmon resonances (LSPRs) in the vicinity of sharp wedges or very small gaps are analytically handled by the Green's function and its derivatives. Consequently the method does not suffer from numerical dispersion or instability due to rapid field variations, as may be the case when using field-based volumetric formulations. Nonetheless, despite of all these advantages, the computational requirements for the solution of realistic large-scale plasmonic problems involving thousands or even millions of nanoparticles are still very high due to the high computational complexity of MoM ( $O(N^2)$  using iterative solvers).

In order to extend the practical applicability of SIE-MoM to larger structures, considerable efforts have been made towards the development of fast, efficient algorithms that can reduce the high costs of MoM in terms of both storage and computer processing time. Specifically, we single out the fast multipole method (FMM) [54] and its variants, the multilevel fast multipole algorithm (MLFMA) [27, 28], and the MLFMA combined with the fast Fourier transform (FFT) [30–32]. Based on Gegenbauer's addition theorem for the homogeneous Green function, the FMM reduces the computational cost to  $O(N^{3/2})$ , whereas its multilevel version achieves  $O(N \log N)$  by incorporating plain and adjoint interpolation schemes for the fields. The FFT extension of the latter (MLFMA-FFT) combines the algorithmic efficiency of MLFMA with the high scalability of FMM-FFT [55] via parallelization, which is optimal when using distributed multicore computer clusters. In MLFMA-FFT the translation stage at the top (coarsest) level of the multilevel Cartesian octree decomposition of the geometry is addressed in terms of a 3D circular convolution per sample of the plane wave expansion (Ewald sphere). The convolution is accelerated in the transformed domain by applying the FFT. By

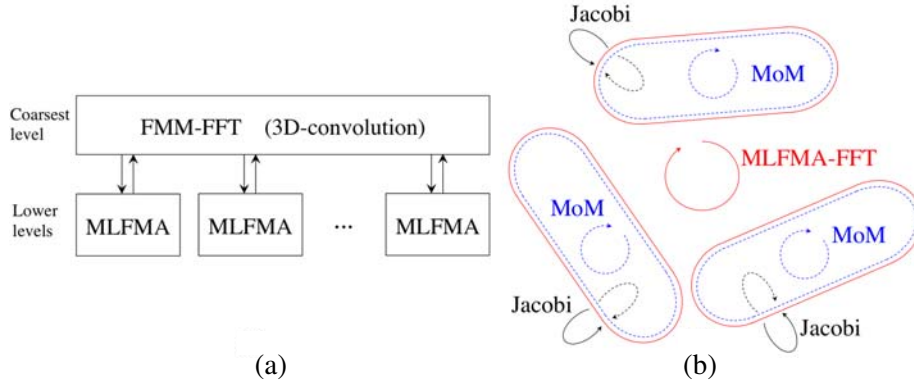


**Figure 6.** (a) Diagram of the MLFMA-FFT distributed algorithm; FMM-FFT is applied at the coarsest level while MLFMA is applied throughout all the lower levels. (b) MLFMA-MoM algorithm; MoM applies for self-couplings through the internal region of the nanoparticles, while MLFMA-FFT applies for the large-scale all-to-all computation through the external region.

so doing, the workload can be distributed among parallel processes by plane wave samples almost without inter-process communication or synchronization (note that the FFT is never parallelized [32]). A schematic description of this method is shown in Fig. 6(a). As an indication of its power, the MLFMA-FFT method has been used to solve an electromagnetic problem with 1 billion unknowns in 2010 [32], and more recently some applications of this methodology to the field of nanoplasmonics can be found in [22].

However, we can still take a step further when dealing with nanoplasmonic applications. Not few nowadays nanotechnology applications revolve around colloidal disordered assemblies of plasmonic nanoparticles or ordered lattices of periodically lined-up nanostructures (metamaterials). In both cases, there is a single (or a few) building element that is repeatedly translated and/or rotated along the structure. When facing such problems with so particular features, the solver should be able to efficiently exploit this repetition pattern. For this we proposed a hybridization of MoM and MLFMA via an efficient strategy for distributing the work [56]. Without lack of generality, let us focus on the case where a single particle is repeated, and let us first consider the problem of the isolated particle in a homogeneous medium. Applying SIE-MoM to this problem poses a matrix system as shown in Equation (26), which according to Equations (24) and (25) can be decomposed into the sum of the contribution of the Green's function through the internal and the external regions simultaneously. Since the nanoparticles are identical except from rotation and translation movements, and thanks to the translational and rotational invariance of the couplings between the basis functions of each particle, the problem can be solved via the hybridization of MoM and MLFMA as follows (see diagram in Fig. 6(b)):

- The calculation of the self-coupling in the internal regions is addressed through MoM. This can be efficiently done with a low computational cost and nearly no memory footprint, given the (comparatively) reduced dimensions of the repeating element.
- The large-scale computation accounting for the self and mutual couplings among all nanoparticles throughout the external region is addressed through MLFMA or MLFMA-FFT in a very efficient manner.
- The block diagonal Jacobi preconditioner [57] can be straightforwardly applied also exploiting the pattern repetition. It is well-known that this preconditioner is extremely suitable in problems with well-separated elements and thus natural splitting of non-adjacent subdomains, such as colloidal or metamaterial systems, leading to fast-converging iterative methods.

#### 4. EXAMPLES

In this section we present some example to demonstrate the accuracy, efficiency and versatility of the above described SIE numerical methods to solve some relevant problems in plasmonics. First we examine

the accuracy of the method by computing the electric near field distribution of a coated silver nanosphere with 50 nm diameter. The shell is made of silica, with a thickness of 25 nm. The silver nanosphere is characterized by the measured frequency-dependent dielectric function taken from [12] for silver, while the silica shell is described by an index of refraction of  $n = 1.456$ , from [58]. The coated sphere is excited by an  $x$ -polarized plane wave with  $\theta_i = 180^\circ$  and an amplitude of 1 V/m at the resonant wavelength of the coated nanoparticle, of 407.5 nm. Figs. 7(a) and (b) show the color maps with the electric near field magnitude in the  $xz$  incident plane containing the polarization of the incident electric field, and the  $xy$  (transversal) plane, respectively. A total of 3,000 unknowns were used to model the electric and magnetic equivalent currents at the vacuum-silica and silica-silver interfaces. Looking at this figure, the penetration of field inside the metallic nanosphere can be clearly observed, while the remarkable electric field enhancement distinctive of LSPRs is obtained inside the Silica shell, at the silica-silver interface. These results are virtually identical to the analytical results provided by the Mie's series [59] (the latter two are not shown for conciseness). The relative root-mean-square (RMS) error for the magnitude of the simulated electric field compared to the analytical field, defined as:

$$e_{\text{RMS}} = \frac{\sqrt{\frac{1}{P} \sum_{p=1}^P |\mathbf{E}_{\text{sim}}(p) - \mathbf{E}_{\text{Mie}}(p)|^2}}{\max(|\mathbf{E}_{\text{Mie}}(p)|)}, \quad (29)$$

where  $\mathbf{E}_{\text{sim}}$  and  $\mathbf{E}_{\text{Mie}}$  are arrays with the simulated and analytical electric field over the  $P$  observation points, is below  $5.27 \cdot 10^{-4}$ .

The large electromagnetic hot spots associated with LSPR excitation give rise to the well-known surface enhanced emission phenomena, which is the bedrock of the Surface Enhanced Raman Scattering (SERS) optical spectroscopy technique [4, 60–63]. Raman spectroscopy has long been an important biosensing method for the specific identification of molecules. Simply put, it involves impinging onto a sample of analyte molecules with a laser source. Of the light that is absorbed by the sample, most of it is elastically scattered back at the same laser wavelength (Rayleigh scattering). However, a very small portion of the impinging energy is inelastically scattered in a range of wavelengths that depends on the energy differences between vibrational states of the molecule. Different molecules have different vibrational modes, so the spectrum of the inelastically scattered light yields a molecular fingerprint which uniquely identifies the interrogated molecule.

The SERS effect results from the very high enhancement of the otherwise extremely weak Raman (inelastic) emission of molecules adsorbed onto arrangements or colloids of metal nanoparticles supporting LSPRs. It has become a powerful spectroscopy technique for the ultrasensitive detection

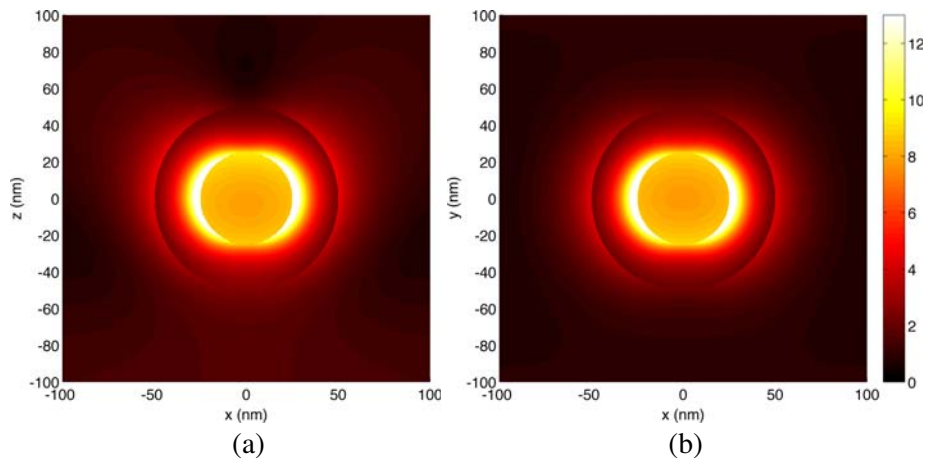


**Figure 7.** Magnitude of the total electric near field for a silver nanosphere coated by a shell of silica and illuminated by an incident  $x$ -polarized plane wave impinging from  $\theta_i = 180^\circ$  at a wavelength of 407.5 nm. (a) Distribution on the  $xz$  (incident) plane. (b) Distribution on the  $xy$  (transversal) plane.

of a variety of organic molecules at low concentrations [23, 64]. Currently, much effort is being put in devising pathways that allow for the detection of small inorganic molecules and ions too [65]. Most of these paths pass through obtaining substrates with higher electromagnetic enhancements that result in even stronger hot spots.

The SERS electromagnetic enhancement factor can be calculated from simulation data as follows [60, 62]:

$$\text{E.F.} = \frac{|\mathbf{E}(\omega_{in})|^2}{|\mathbf{E}_i(\omega_{in})|^2} \frac{|\mathbf{E}(\omega_{out})|^2}{|\mathbf{E}_i(\omega_{out})|^2}, \quad (30)$$

where  $\mathbf{E}_i$  is the electric field of the incident laser source and  $\mathbf{E}$  the total field in the presence of the nanoparticle enhancement system. The first term in Equation (30) represents the local electric field intensity enhancement at the incident frequency  $\omega_{in}$ . The second term represents the local electric field intensity enhancement of the Raman inelastic scattering from the interrogated molecule. Note that the calculation of the second term rests on the application of the reciprocity theorem, by repeating the simulation under a laser light excitation at the Raman-shifted (output) frequency  $\omega_{out}$ . When the Raman shift is small compared with  $\omega_{in}$ , or in order to estimate the potential enhancement in a given system, the SERS enhancement factor can be approximated as  $\text{E.F.} \approx |\mathbf{E}(\omega_{in})|^4 / |\mathbf{E}_i(\omega_{in})|^4$ , which poses a fourth power dependence on the local electric field enhancement. This is why very high enhancements can be obtained using this technique.

Figure 8(a) shows an example of SERS for a colloidal deposition of 2,900 gold nanorods (NRs) compacted in a  $1 \times 1 \mu\text{m}^2$  monolayer with a minimum interparticle separation of 1 nm. A zoom on the central region of this figure is shown in Fig. 8(b). The NRs have a diameter of 17.5 nm, a length of 54 nm, and they are ended with hemispherical end-caps. The SERS enhancement factor is calculated as  $|\mathbf{E}(\omega_{in})|^4 / |\mathbf{E}_i^{\text{max}}(\omega_{in})|^4$  for a highly focused laser illumination at normal incidence and linear  $\hat{y}$ -polarization. The beam is focused by an aplanatic optical lens [62] with numerical aperture  $\text{NA} = 0.7$ , focal length of 4 mm and very large filling factor. The incident wavelength is  $\lambda_{in} = 785 \text{ nm}$ , in accordance with usual experimental setups.  $|\mathbf{E}_i^{\text{max}}(\omega_{in})|$  is the maximum field strength at the center of the lens focus. Very high enhancement factors  $> 10^8$  can be observed at the center region, coinciding with the location of the lens focus.

The simulations were carried out on a workstation with 4 Intel Xeon E7-8880v2 microprocessors, each with 15 cores clocked at 2.50 GHz, which gives 60 physical processors overall (no hyperthreading is used). The total memory and execution time needed to compute  $\mathbf{E}(\omega_{in})$  was of 110.03 GB and 5.5 hours. The total number of unknowns required to solve the whole system was 7.08 million.

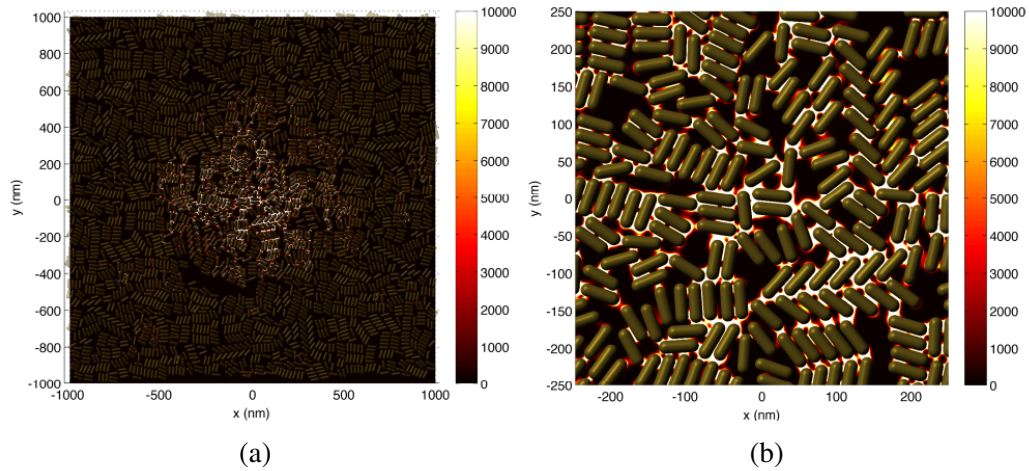


**Figure 8.** (a) SERS on an in-vacuum colloidal deposition of 2,900 gold nanorods (NRs) compacted in a  $1 \times 1 \mu\text{m}^2$  monolayer (minimum interparticle separation of 1 nm) irradiated by a highly focused laser beam at 785 nm. (b) Zoom on the central region of the SERS color map distribution.

## 5. CONCLUSION

Plasmonic nanoparticles play an important role in biomedical applications as they can serve as bioimaging agents, be employed in biosensor devices for the early diagnosis of diseases, and exhibit promising results in vivo as therapeutic agents. This is because of their plasmonic properties, originated from the interaction of such small particles with electromagnetic irradiation that gives rise to the localized surface plasmons (collective oscillations of their surface conduction electrons). The quanta of these oscillations are known as plasmons, and their frequency increases with the electron density. The optical response of plasmonic metals is generally well-described by classical electrodynamics. The theoretical understanding of plasmons and the design of plasmonic nanostructures can therefore directly benefit from knowledge gathered in electrical engineering, antenna design, and other classical areas in which the solution of the electromagnetic problems plays a central role. In recent works, the most computationally efficient approaches in computational electromagnetics comprising SIE formulations based on the Maxwell's Equations, combined with the MoM and the most recent advances in spectral acceleration techniques based on MLFMA, have been successfully applied to model realistic plasmonic problems. Although not yet widespread in optics, these methods bring important advantages when compared to the previously used volumetric approaches. Thus, in the context of the commemoration on 150 Years of Maxwell's Equations, this paper has been devoted to review the ultimate advances in nanoplasmonic modeling, showing those SIE methods that have extended the scope of application of Maxwell's Equations from microwave to optical frequency bands, illustrating how they have allowed/achieved the accurate simulation of real-life plasmonic problems that can be straightforwardly applied to the solution of cutting-edge medical biosensing nanoscience challenges.

## ACKNOWLEDGMENT

This work was supported by the European Regional Development Fund (ERDF) and the Spanish Ministerio de Economía y Competitividad (Projects MAT2014-58201-C2-1-R, MAT2014-58201-C2-2-R, Project TACTICA), from the ERDF and the Galician Regional Government under Projects CN2012/279 and CN2012/260 (AtlantTIC) and the Plan I2C (20112015), and from the ERDF and the Extremadura Regional Government (Junta de Extremadura) under Project IB13185.

## REFERENCES

1. "Nature milestones: Photons supplement," 2010, <http://www.nature.com/milestones/photons>.
2. O'Neal, D. P., L. R. Hirsch, N. J. Halas, J. D. Payne, and J. L. West, "Photo-thermal tumor ablation in mice using near infrared-absorbing nanoparticles," *Cancer Lett.*, Vol. 209, 171–176, 2004.
3. Oulton, R. F., V. J. Sorger, T. Zentgraf, R. M. Ma, C. Gladden, L. Dai, G. Bartal, and X. Zhang, "Plasmon lasers at deep subwavelength scale," *Nature*, Vol. 461, 629–632, 2009.
4. Alvarez-Puebla, R. A. and L. M. Liz-Marzn, "SERS-based diagnosis and biodetection," *Small*, Vol. 6, No. 5, 604–610, 2010.
5. Atwater, H. A. and A. Polman, "Plasmonics for improved photovoltaic devices," *Nat. Mater.*, Vol. 9, 205–213, 2010.
6. Noginov, M. A., G. Zhu, A. M. Belgrave, R. Bakker, V. M. Shalaev, E. E. Narimanov, S. Stout, E. Herz, T. Suteewong, and U. Wiesner, "Demonstration of a spaser-based nanolaser," *Nature*, Vol. 460, 1110–1113, 2009.
7. Akimov, A. V., A. Mukherjee, C. L. Yu, D. E. Chang, A. S. Zibrov, P. R. Hemmer, H. Park, and M. D. Lukin, "Generation of single optical plasmons in metallic nanowires coupled to quantum dots," *Nature*, Vol. 450, 402–406, 2007.
8. Alù, A. and N. Engheta, "Wireless at the nanoscale: Optical interconnects using matched nanoantennas," *Phys. Rev. Lett.*, Vol. 104, 213902, 2010.
9. Atwater, H. A., "The promise of plasmonics," *Scientific American*, Vol. 296, No. 4, 56–62, 2007.
10. Maier, S. A., *Plasmonics: Fundamentals and Applications*, Springer, New York, 2010.

11. Jackson, J. D., *Classical Electrodynamics*, Wiley, New York, 1962.
12. Johnson, P. B. and R. W. Christy, "Optical constants of the noble metals," *Phys. Rev. B*, Vol. 6, No. 12, 4370–4379, 1972.
13. Palik, E. D., *Handbook of Optical Constants of Solids*, Academic Press, New York, 1985.
14. García de Abajo, F. J., "Nonlocal effects in the plasmons of strongly interacting nanoparticles, dimers, and waveguides," *J. Phys. Chem. C*, Vol. 112, No. 46, 17983–17987, 2008.
15. Draine, B. T., "The discrete-dipole approximation and its application to interstellargraphite grains," *Astrophys. J.*, Vol. 333, 848–872, 1988.
16. Taflove, A. and M. E. Brodwin, "Numerical solution of steady-state electromagnetic scattering problems using the time-dependent Maxwell's equations," *IEEE Trans. Microwave Theory Tech.*, Vol. 23, 623–630, 1975.
17. Hao, F., C. L. Nehl, J. H. Hafner, and P. Nordlander, "Plasmon resonances of a gold nanostar," *Nano Lett.*, Vol. 7, 729–732, 2007.
18. Jin, J., *The Finite Element Method in Electromagnetics*, Wiley, New York, 2002.
19. Zhang, S., K. Bao, N. J. Halas, H. Xu, and P. Nordlander, "Substrate-induced fano resonances of a plasmonic nanocube: A route to increased-sensitivity localized surface plasmon resonance sensors revealed," *Nano Lett.*, Vol. 11, 1657–1663, 2011.
20. Harrington, R. F., *Field Computation by Moment Method*, IEEE Press, New York, 1993.
21. Taboada, J. M., J. Rivero, F. Obelleiro, M. G. Araújo, and L. Landesa, "Method-of-moments formulation for the analysis of plasmonic nano-optical antennas," *J. Opt. Soc. Am. A*, Vol. 28, 1341–1348, 2011.
22. Solís, D. M., J. M. Taboada, F. Obelleiro, L. M. Liz-Marzán, and F. J. García de Abajo, "Toward ultimate nanoplasmonics modeling," *ACS Nano*, Vol. 8, 7559–7570, 2014.
23. Hamon, C., S. M. Novikov, L. Scarabelli, D. M. Solís, T. Altantzis, S. Bals, J. M. Taboada, F. Obelleiro, and L. M. Liz-Marzán, "Collective plasmonic properties in few-layer gold nanorod supercrystals," *ACS Photonics*, Vol. 2, No. 10, 1482–1488, 2015.
24. Araújo, M. G., J. M. Taboada, D. M. Solís, J. Rivero, L. Landesa, and F. Obelleiro, "Comparison of surface integral equation formulations for electromagnetic analysis of plasmonic nanoscatterers," *Optics Express*, Vol. 20, No. 8, 9161–9171, 2012.
25. Solís, D. M., J. M. Taboada, and F. Obelleiro, "Surface integral equation method of moments with multiregion basis functions applied to plasmonics," *IEEE Trans. Antennas Propag.*, Vol. 63, No. 5, 2141–2152, 2015.
26. Solís, D. M., J. M. Taboada, O. Rubiños-López, and F. Obelleiro, "Improved combined tangential formulation for electromagnetic analysis of penetrable bodies," *JOSA B*, Vol. 32, No. 9, 1780–1787, 2015.
27. Song, J. M., C. C. Lu, and W. C. Chew, "Multilevel fast multipole algorithm for electromagnetic scattering by large complex objects," *IEEE Trans. Antennas Propag.*, Vol. 45, 1488–1493, 1997.
28. Donepudi, K. C., J.-M. Jin, and W. C. Chew, "A higher order multilevel fast multipole algorithm for scattering from mixed conducting/dielectric bodies," *IEEE Trans. Antennas Propag.*, Vol. 51, No. 10, 2814–2821, 2003.
29. Araújo, M. G., D. M. Solís, J. Rivero, J. M. Taboada, and F. Obelleiro, "Solution of large-scale plasmonic problems with the multilevel fast multipole algorithm," *Optics Letters*, Vol. 37, No. 3, 416–418, 2012.
30. Taboada, J. M., M. G. Araújo, J. M. Bértolo, L. Landesa, F. Obelleiro, and J. L. Rodríguez, "MLFMA-FFT parallel algorithm for the solution of large-scale problems in electromagnetics (Invited Paper)," *Progress In Electromagnetics Research*, Vol. 105, 15–30, 2010.
31. Araújo, M. G., J. M. Taboada, F. Obelleiro, J. M. Bértolo, L. Landesa, J. Rivero, and J. L. Rodríguez, "Supercomputer aware approach for the solution of challenging electromagnetic problems," *Progress In Electromagnetics Research*, Vol. 101, 241–256, 2010.
32. Taboada, J. M., M. G. Araújo, F. Obelleiro, J. L. Rodríguez, and L. Landesa, "MLFMA-FFT parallel algorithm for the solution of extremely large problems in electromagnetics," *Proceedings of*

- the IEEE, Special issue on Large Scale Electromagnetic Computation for Modeling and Applications*, Vol. 101, No. 2, 350–363, 2013.
33. Solís, D. M., J. M. Taboada, M. G. Araújo, F. Obelleiro, and J. O. Rubiños-López, “Design of optical wide-band log-periodic nanoantennas using surface integral equation techniques,” *Opt. Commun.*, Vol. 301–302, 6166, 2013.
  34. Obelleiro, F., J. M. Taboada, D. M. Solís, and L. Bote, “Directive antenna nanocoupler to plasmonic gap waveguides,” *Opt. Lett.*, Vol. 38, 1630–1632, 2013.
  35. Solís, D. M., J. M. Taboada, F. Obelleiro, and L. Landesa, “Optimization of an optical wireless nanolink using directive nanoantennas,” *Opt. Express*, Vol. 21, 2369–2377, 2013.
  36. Farrokhtakin, E., D. Rodríguez-Fernández, V. Mattoli, D. M. Solís, J. M. Taboada, F. Obelleiro, M. Grzelczak, and L. M. Liz-Marzán, “Radial growth of plasmon coupled gold nanowires on colloidal templates”, *Journal of Colloid and Interface Science*, Vol. 449, 87–91, 2015.
  37. Fernández-López, C., L. Polavarapu, D. M. Solís, J. M. Taboada, F. Obelleiro, R. Contreras-Caceres, I. Pastoriza-Santos, and J. Perez-Juste, “Gold nanorods-pNIPAM hybrids with reversible plasmon coupling: Synthesis, modeling and sers properties,” *ACS Applied Materials & Interfaces*, Vol. 7, No. 23, 12530–12538, 2015.
  38. Shiohara, A., S. M. Novikov, D. M. Solís, J. M. Taboada, F. Obelleiro, and L. M. Liz-Marzán, “Plasmon modes and hot spots in gold nanostarsatellite clusters,” *Journal of Physical Chemistry C*, Vol. 119, No. 20, 10836–10843, 2015.
  39. Drude, P., “Zur elektronentheorie der metalle,” *Ann. Phys.*, Vol. 306, No. 3, 566–613, 1900.
  40. Vial, A., A.-S. Grimault, D. Macías, D. Barchiesi, and M. Lamy de la Chapelle, “Improved analytical fit of gold dispersion: Application to the modeling of extinction spectra with a finite-difference time-domain method,” *Phys. Rev. B*, Vol. 71, No. 8, 085416, 2005.
  41. Ritchie, R. H., “Plasma losses by fast electrons in thin films,” *Phys. Rev.*, Vol. 106, No. 5, 874–881, 1957.
  42. Ylä-Oijala, P., M. Taskinen, and S. Järvenpää, “Surface integral equation formulations for solving electromagnetic scattering problems with iterative methods,” *Radio Sci.*, Vol. 40, No. 6, 1–19, 2005.
  43. Rao, S. M., D. R. Wilton, and A. W. Glisson, “Electromagnetic scattering by surfaces of arbitrary shape,” *IEEE Trans. Antennas Propag.*, Vol. 30, No. 3, 409–418, 1982.
  44. Wilton, D. R., S. M. Rao, A. W. Glisson, D. H. Schaubert, O. M. Al-Bundak, and C. M. Butler, “Potential integrals for uniform and linear source distributions on polygonal and polyhedral domains,” *IEEE Trans. Antennas Propag.*, Vol. 32, 276–281, 1984.
  45. Hodges, R. E. and Y. Rahmat-Samii, “The evaluation of MFIE integrals with the use of vector triangle basis functions,” *Microwave Opt. Technol. Lett.*, Vol. 14, 9–14, 1997.
  46. Graglia, R. D., “On the numerical integration of the linear shape functions times the 3-D Greens function or its gradient on a plane triangle,” *IEEE Trans. Antennas Propag.*, Vol. 41, 1448–1455, 1993.
  47. Ylä-Oijala, P. and M. Taskinen, “Calculation of CFIE impedance matrix elements with RWG and nxRWG functions,” *IEEE Trans. Antennas Propag.*, Vol. 51, 1837–1846, 2003.
  48. Kahan, W., “Branch cuts for complex elementary functions, or much ado about nothing’s sign bit,” *The State of the Art in Numerical Analysis*, A. Iserles and M. J. D. Powell, eds., Clarendon Press, Oxford, 1987.
  49. Ziolkowski, R. W. and E. Heyman, “Wave propagation in media having negative permittivity and permeability,” *Phys. Rev. E Stat. Nonlin. Soft Matter Phys.*, Vol. 64, No. 5, 056625, 2001.
  50. *Standard C++ Library Reference*, IBM Corp., 2005.
  51. Obelleiro, F., J. M. Taboada, and M. G. Araújo, “Calculation of wave propagation parameters in generalized media,” *Microwave Opt. Technol. Lett.*, Vol. 54, No. 12, 2731–2736, 2012.
  52. Putnam, J. M. and L. N. Medgyesi-Mitschang, “Combined field integral equation formulation for inhomogeneous two- and three-dimensional bodies: The junction problem,” *IEEE Trans. Antennas Propag.*, Vol. 39, No. 5, 667–672, 1991.

53. Ylä-Oijala, P., M. Taskinen, and J. Sarvas, "Surface integral equation method for general composite metallic and dielectric structures with junctions," *Progress In Electromagnetics Research*, Vol. 52, 81–108, 2005.
54. Coifman, R., V. Rokhlin, and S. Wanzura, "The fast multipole method for the wave equation: A pedestrian prescription," *IEEE Antennas Propag. Mag.*, Vol. 35, 7–12, 1993.
55. Waltz, C., K. Sertel, M. A. Carr, B. C. Usner, and J. L. Volakis, "Massively parallel fast multipole method solutions of large electromagnetic scattering problems," *IEEE Trans. Antennas Propag.*, Vol. 55, No. 6, 1810–1816, 2007.
56. Sols, D. M., M. G. Arajo, L. Landesa, S. Garca, J. M. Taboada, and F. Obelleiro, "MLFMA-MoM for solving the scattering of densely packed plasmonic nanoparticle assemblies," *IEEE Photonics Journal*, Vol. 7, No. 3, 4800709, 2015.
57. Saad, Y., *Iterative Methods for Sparse Linear Systems*, PWS, Boston, 1996.
58. Philipse, A. P. and A. Vrij, "Preparation and properties of nonaqueous model dispersions of chemically modified, charged silica spheres," *J. Colloid Interface Sci.*, Vol. 128, 121–136, 1989.
59. Mie, G., "Beitrgе zur optik truber medien, speziell kolloidaler metallungen," *Ann. Phys. Leipzig, Ger.*, Vol. 25, 377–445, 1908.
60. Metiu, H., "Surface enhanced spectroscopy," *Prog. Surf. Sci.*, Vol. 17, 153–320, 1984.
61. Moskovits, M., "Surface-enhanced spectroscopy," *Rev. Mod. Phys.*, Vol. 57, 783, 1985.
62. Novotny, L. and B. Hecht, *Principles of Nano-Optics*, Cambridge Univ. Press, Cambridge, 2006.
63. Schlücker, S., "Surface-enhanced raman spectroscopy: Concepts and chemical applications," *Angew. Chem., Int. Ed.*, Vol. 53, 4756–4795, 2014.
64. Alvarez-Puebla, R. A., A. Agarwal, P. Manna, B. P. Khanal, P. Aldeanueva-Potel, E. Carb-Argibay, N. Pazos-Prez, L. Vigderman, E. R. Zubarev, N. A. Kotov, and L. M. Liz-Marzn, "Gold nanorods 3D-supercrystals as SERS substrates for the rapid detection of scrambled prions," *Proc. Natl. Acad. Sci. U.S.A.*, Vol. 108, 8157–8161, 2011.
65. Alvarez-Puebla, R. A. and L. M. Liz-Marzn, "SERS detection of small inorganic molecules and ions," *Angew. Chem. Int. Ed.*, Vol. 51, 11214–11223, 2012.